Correlations between wind stress and significant wave height in the Bay of Bengal region

Susmita Biswas[1*]

[1*]Department of Cyber Science & Technology Brainware University Barasat, West Bengal, Kolkata-124 bi.susmita@gmail.com

Abstract – Prediction of significant wave height (Swh) and Wind stress (WS) were carried out spatially and temporally for a period of nine years (2015-2023) in the Bay of Bengal (BOB) region using a combination of empirical orthogonal function (EOF) analysis. In the present work, WAM-4C model is performed to generate spatially gridded swh data for nine years (2015-23). Six hourly NCEP blended winds have been applied to force the model. The wind stress, is estimated from wind speed using a drag coefficient. Then Swh and WS are reconstructed using the first six dominant EOFs and corresponding PCs (principal components). Spatial correlation is evaluated between model computed swh and WS and reconstructed Swh and WS for January and July 2023. It is concluded that the temporal variations are compared for the Swh and the WS parameters. Establishment of Linear relations are in between Swh and WS for the BOB region for all the nine years and also particular months of a year.

Keywords - Wind stress; Significant wave height; Bay of Bengal; EOF analysis; Reconstruction.

I. INTRODUCTION

Wind stress at the air-sea interface has a significant influence on wind-wave interaction and is thought to be a critical parameter in describing many of the temporal and spatial signatures on the ocean surface, prompting numerous experimental and analytical studies. [1] investigated wind stress as a function of both wind speed and significant wave height. He discovered that increasing wave height reduces wind stress at a constant speed, as does the curvature of wind profile.

Wind stress and drag coefficient of ocean surface are very critical parameters in the research of ocean and atmospheric dynamics especially in that of air-sea interaction. The horizontal force of the wind on the sea surface is called the wind stress. It represents the vertical transmission of horizontal motion. Wind stress transfers momentum from the atmosphere to the water. The momentum exchange caused by wind stress at the atmosphere-ocean interface is important for a variety of reasons, including air-sea interaction research, climate studies, ocean modelling, and ocean prediction on several time periods. The total wind stress magnitude (T) at the ocean surface is calculated from the square of the wind speed at 10 m above the sea surface (U), the density of air (ρ_a), and a dimensionless drag coefficient (C_D) using $T = \rho_a C_D U^2$ [2]. Turbulent energy fluxes are proportional to U. The change in fluxes due to the change in U is easily estimated.

EOFs are used to obtain dominant patterns of ocean variations spatially and to reduce the dimensionality of the data. The EOF analysis is earlier used by [5] and [6] over the Indian Ocean to understand the variability of surface fluxes and wind stress curl. Recent studies of [8, 9] and [3] have demonstrated wind forecast techniques using EOF analysis in conjunction with genetic algorithm on satellite scatterometer derived winds for the AS, BOB and north Indian Ocean regions separately. [7] studied spatial-temporal variability of SWH over the Indian Ocean by dividing it into four regions. In the present work model generated Swh data and calculated WS data is analyzed spatially and temporally for the BOB region and then explored for possible relationship between them.

II. DATA

The WAM model [10] is operationally used for forecasting sea state on global and regional scales. It is a third-generation model in which the two-dimensional ocean wave spectrums are computed by integration of the energy balance equation without any prior restriction on the spectral shape. The model is continuously updated, the version being used here is cycle 4, known as WAM-4C as given by [4]. WAM-4C is used in the present study and is integrated for the period 2015-23 covering the BOB area 77°E to 102°E and 24°N to 6°N. For this study, we have used 6-hourly, and 0.5-degree QSCAT/NCEP blended ocean winds from Colorado Research Associates as forcing to the model. Bathymetry is derived from ETOPO5.

The squared correlation coefficient improved to 0.88 in January 2023 and a high of 0.91 in July 2023. Thus, it is concluded linear relationship with very high positive relation between SWH and WS in the month of July for the BOB region.

Wind stress *T* is calculated from

$$T = \rho_a C_D U_{10}^2$$

where ρ_a= 1.3kg/m^3 is the density of air, U_{10} is wind speed at 10 meters, and C_D is the drag coefficient.

III. RESULTS AND DISCUSSIONS

EOF analysis is carried out across the BOB region for nine years (2015-2023) using model computed Swh and calculated wind stress (WS). The first six eigenvectors collectively account for 92% of the total variability in Swh and 55% of the total variability in WS. The first EOF accounts for 76.6% and the second EOF for 8% of the total variance for the Swh field. Similarly, the first EOF accounts for 36.5% and the second EOF for .6% of the total variance for the WS field. From the first spatial mode (EOF1) of WS depicted in Figure 1a, it can see that the maximum amplitude is observed in the central BOB. EOF1 of Swh depicted in Figure 1b gives the maximum amplitude in the northeast BOB.

The maximum loading occurs in the northeast corner of the bay since during the southwest monsoon the dominant direction of propagation of the waves is northeastward. Next the Swh and WS is reconstructed using original first six EOFs and corresponding PCs. Figures 2a and 2b shows the model computed Swh for January 2023 and reconstructed Swh using EOFs and PCs for the same period. Figures 3a and 3b show similar plots for WS data for January 2023. We conclude reasonable accuracy of the reconstructed parameters. Finally, spatial correlation was evaluated between model computed Swh and WS and reconstructed Swh and WS for January 2023. Figures 4a and 4b shows high positive correlation along the east coast of India. Figures 5a and 5b shows the model computed Swh for July 2023 and reconstructed Swh using EOFs and PCs. For July 2023 figures 6a and 6b depicts computed and reconstructed WS. Again, there is reasonable accuracy of the reconstruction. Figures 7a and 7b shows high positive correlation almost in the entire BOB region between model computed Swh and WS and reconstructed Swh and WS for July 2023. Figure 8 depicts the PC1 of Swh and WS for the period 2015-2023. The Swh data exhibits yearly periodicity, with a maximum occurring during the southwest monsoon season. The PC1 of WS data follows a similar pattern, albeit with decreased amplitudes. Figures 9a and 9b depict scatter plots of PC1 of Swh and WS for the period 2015-2023 and solely for the year 2015. There is a linear association with squared correlation coefficients more than 0.6 in both situations. Finally, figures 10a and 10b show scatter plots of PC1 of Swh and WS for January and July 2015, respectively.

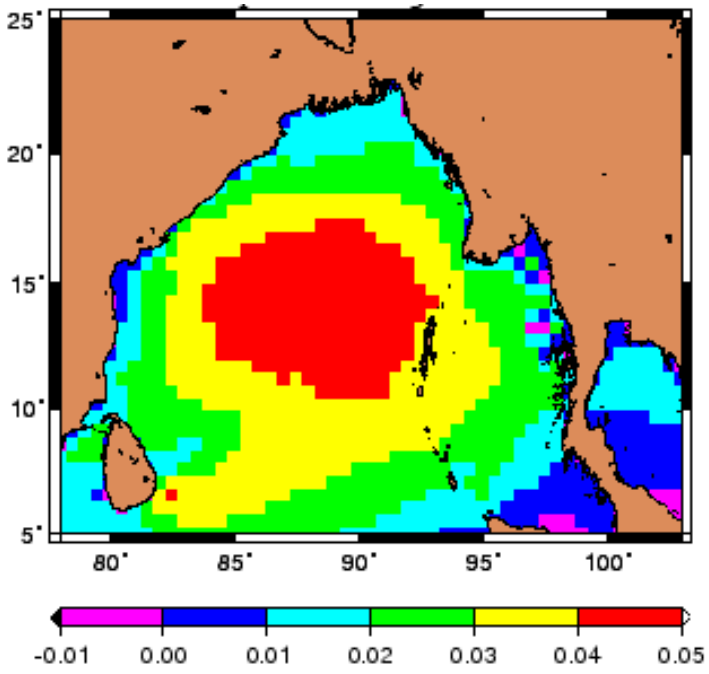

Fig. 1(a). First EOF of WS

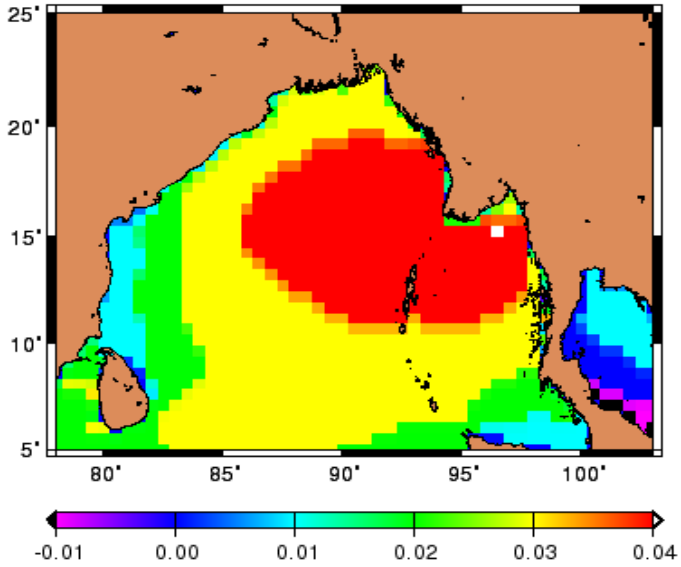

Fig. 1(b). First EOF of SWH

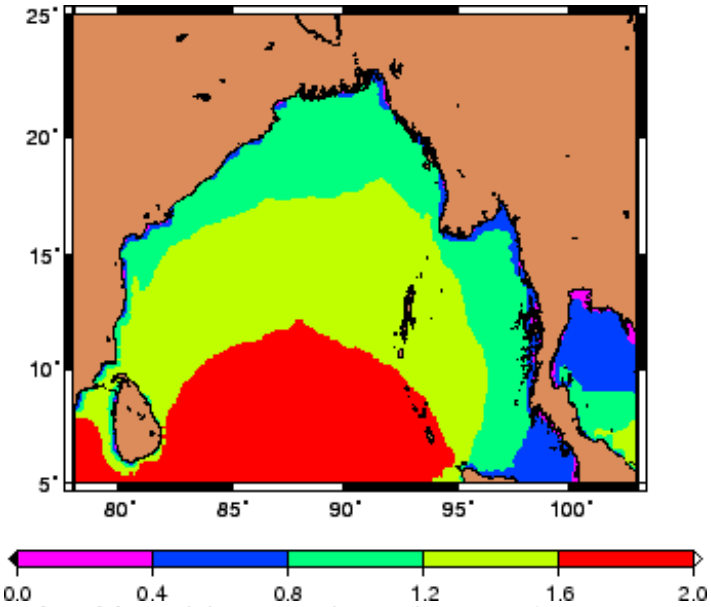

Fig. 2(a). Model computed SWH in meters for JAN 2023

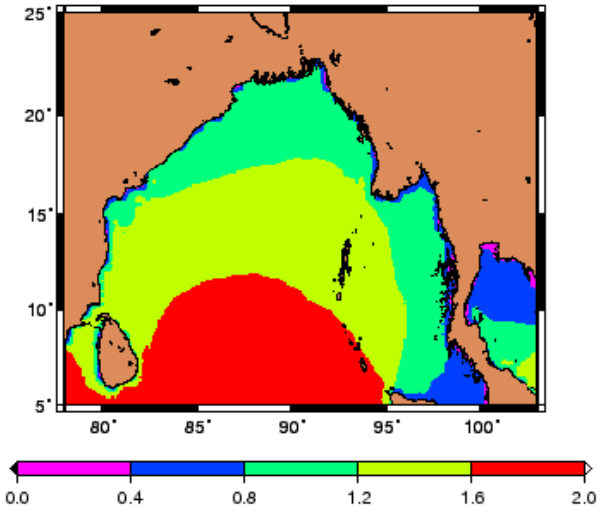

Fig. 2(b). Reconstructed SWH in meters using EOFs and PCs for JAN 2023.

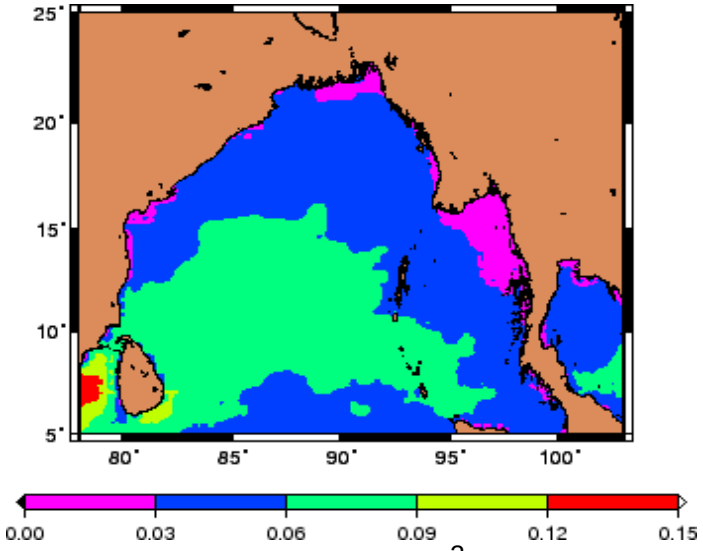

Fig. 3(a). Computed WS in N/m^2 for JAN 2023

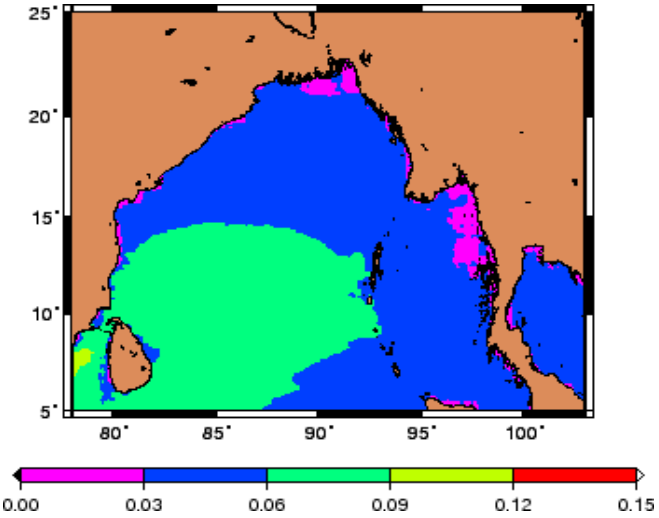

Fig. 3(b). Reconstructed WS in N/m^2 using EOFs and PCs for JAN 2023.

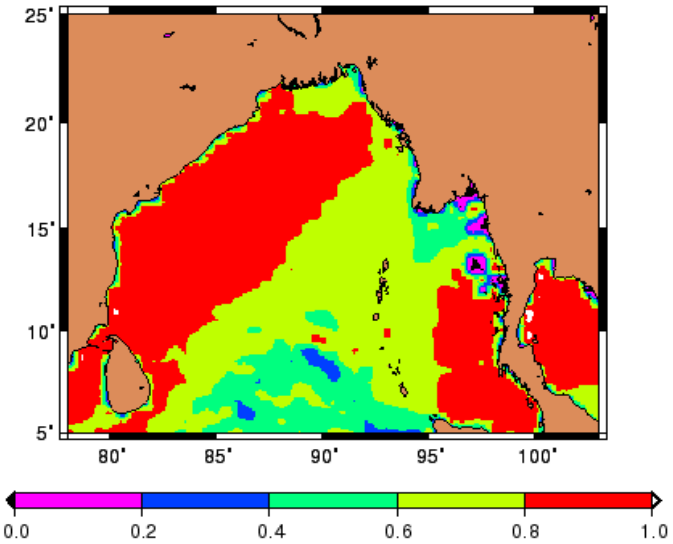

Fig. 4(a). Correlation between model computed SWH and WS for JAN 2023

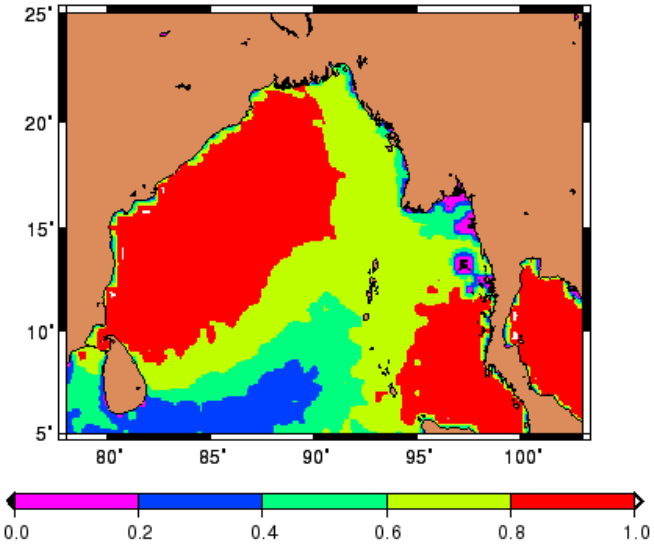

Fig. 4(b). Correlation between reconstructed SWH and WS using EOFs and PCs for JAN 2023.

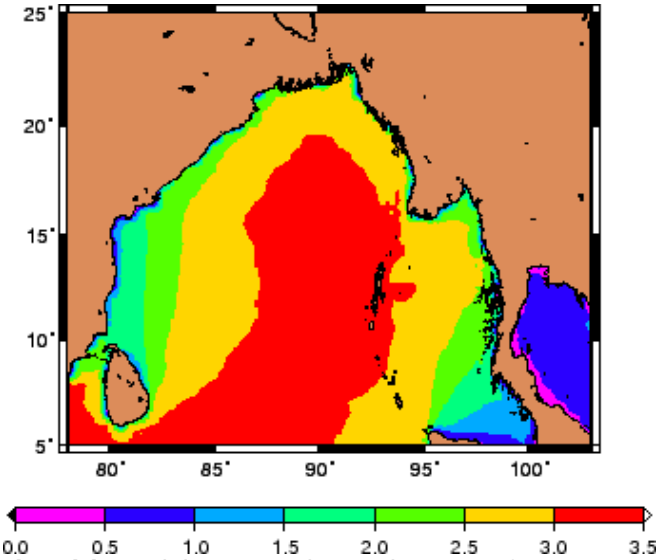

Fig. 5(a). Model computed SWH in meters for JUL 2023

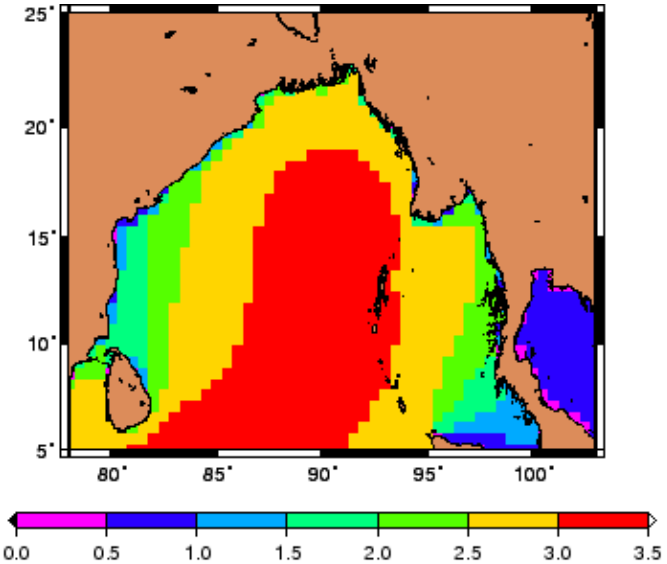

Fig. 5(b). Reconstructed SWH in meters using EOFs and PCs for JUL 2023.

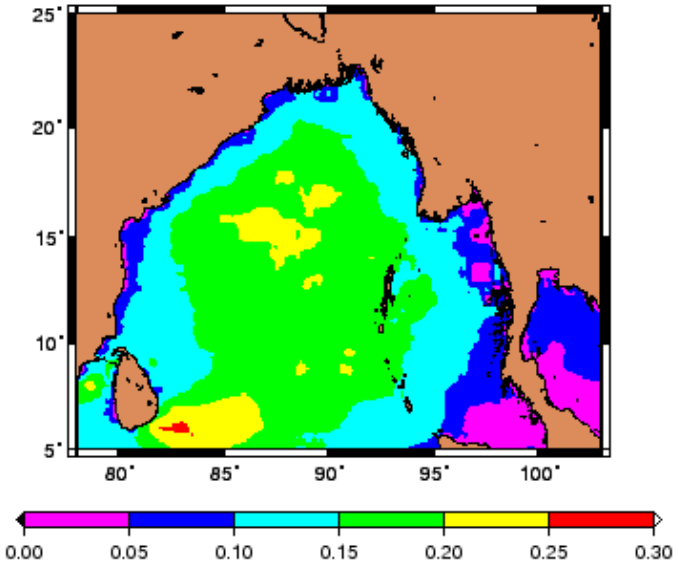

Fig. 6(a). Computed WS in N/m^2 for JUL 2023

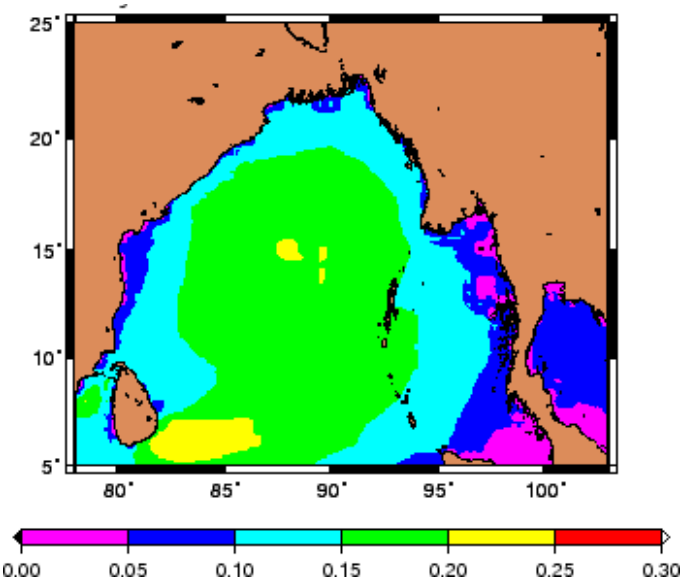

Fig. 6(b). Reconstructed WS in N/m^2 using EOFs and PCs for JUL 2023.

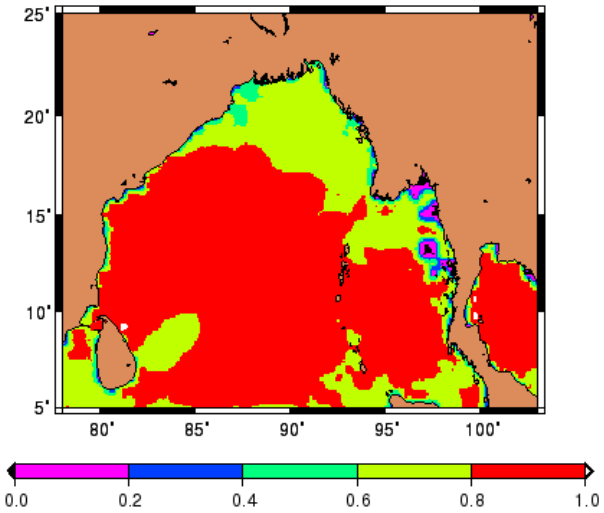

Fig. 7(a). Relationship between model computed SWH and WS for JUL 2023

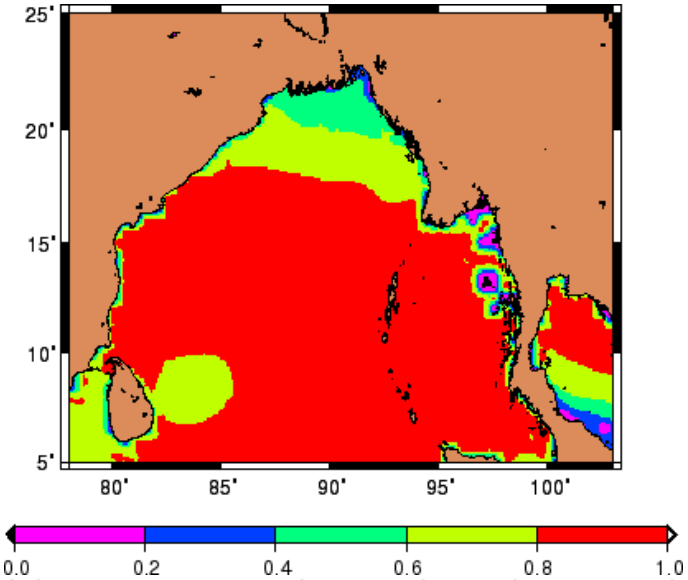

Fig. 7(b). Relatioship between reconstructed SWH and WS using EOFs and PCs for JUL 2023.

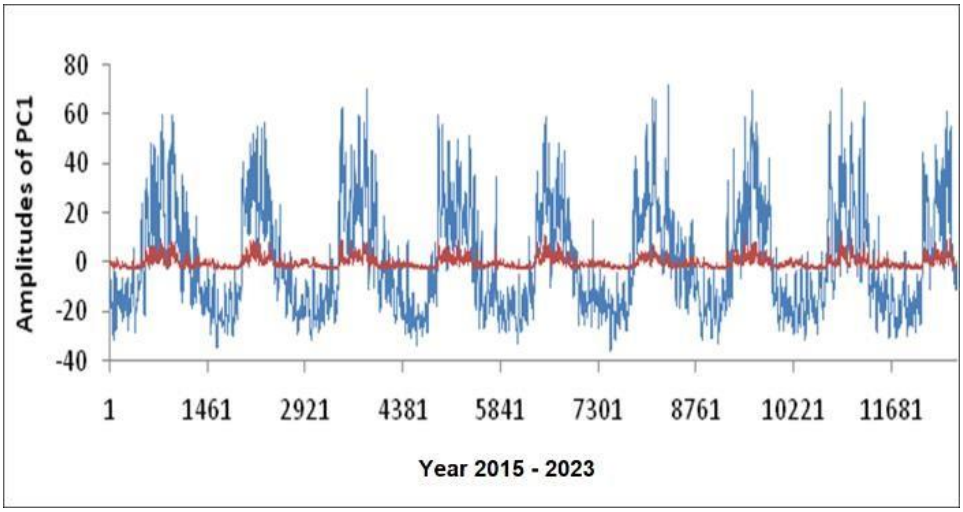

Fig. 8. PC1 of SWH & WS for the period 2015-2023

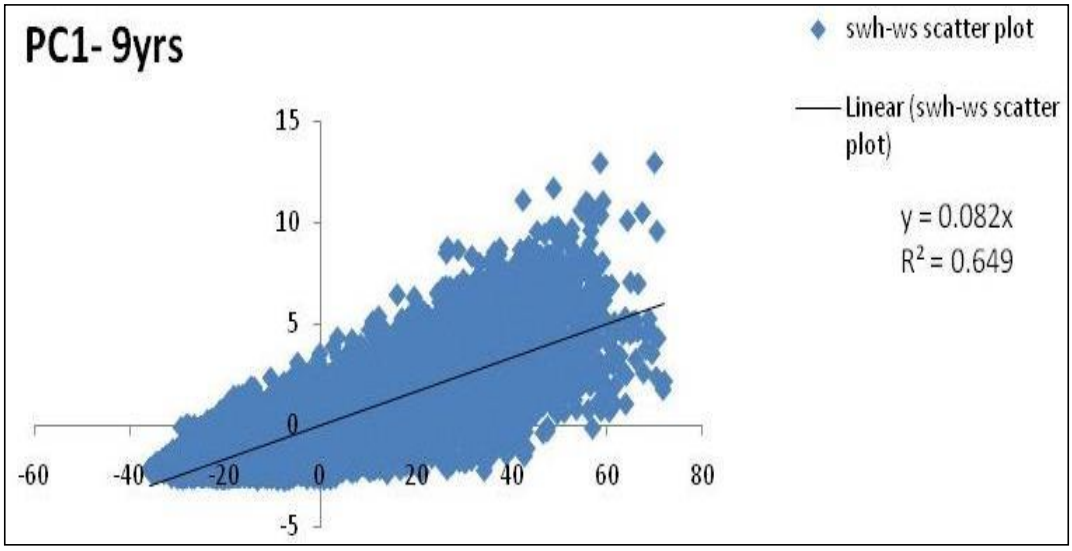

Fig. 9(a). Scatter plot between PC1 of SWH and WS for the period 2015-2023

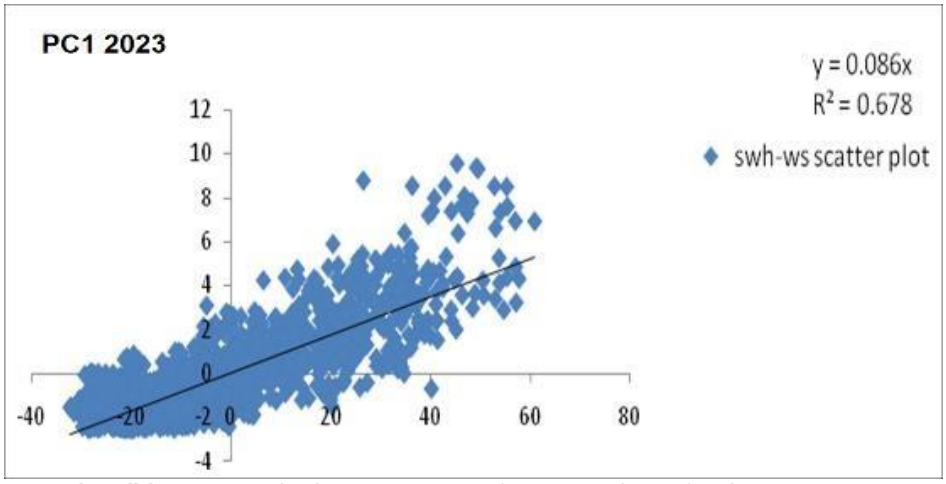

Fig 9(b). Scatter plot between PC1 of SWH and WS for the year 2023

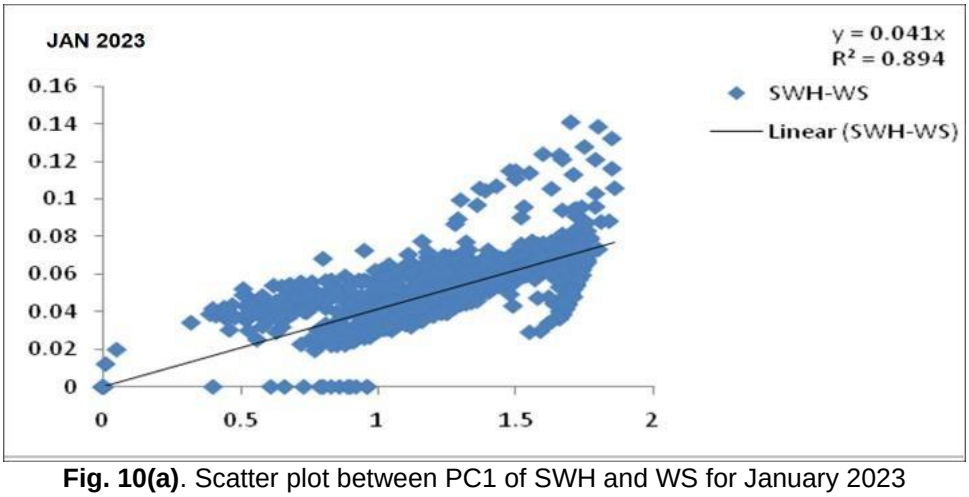

Fig. 10(a). Scatter plot between PC1 of SWH and WS for January 2023

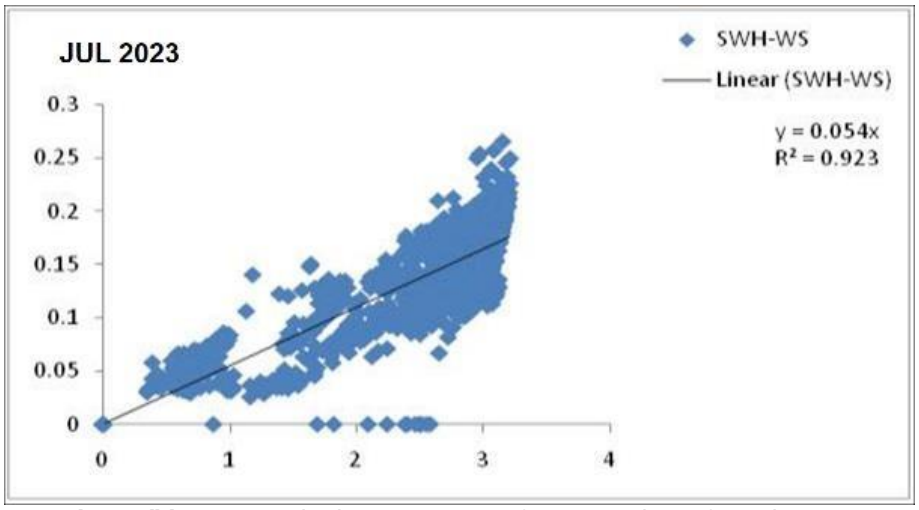

Fig. 10(b). Scatter plot between PC1 of SWH and WS for July 2023

IV. CONCLUSIONS

Swh data for the BOB area are derived using WAM-4C, with WS data calculated for the period 2015-2023. Then, both data sets were submitted to EOF analysis to determine the major modes of variability. The geographical structure of the initial EOF for the BOB region reveals the largest loading in the northeast bay for Swh and the centre bay for WS. The temporal fluctuations have a yearly periodicity. The Swh and WS are rebuilt using the first six EOFs and related PCs. Spatial correlations are determined between model-calculated Swh and WS and reconstructed Swh and WS.

In January 2023, there is a high positive connection along India's east coast, and in July 2023, there is a high positive correlation practically everywhere in the BOB area. Swh and WS have a linear connection from 2015 to 2023, with a squared correlation value greater than 0.6. The association is greater between January and July 2023, with the greatest occurring in July.

References

[1] Blake, R. A., 1991, The dependence of wind stress on wave height and wind speed. J. Geophy. Res. 96: 20531- 20545.

[2] Fairall, C. W., E. F. Bradley, J. E. Hare, A. A. Grachev, and J. B. Edson, 2003, Bulk parameterization of air-sea fluxes: Updates and verification for the COARE algorithm, J. Clim., 16, 571–591.

[3] Basu, S., R. Sharma, N. Agarwal, R. Kumar, and A. Sarkar, 2009, Forecasting of scatterometer-derived wind fields in the north Indian Ocean with a data- adaptive approach, J. Geophys. Res., 114, doi:10.1029/2023JC005201.

[4] Gunther, H., K. Hasselmann and P.A.E.M. Janssen, Report No.4, The WAM Model Cycle 4, Hamburg, 1992.

[5] Jones, C. S., D. M. Légler, and J. O'Brien, 1995, Variability of surface fluxes over the Indian Ocean: 1960-1989, The Global Atmosphere and Ocean System, 3, 249-272.

[6] Rao, A. D., 2002, Variability of wind stress curl over the Indian Ocean during years 1970-1995, Indian Journal of Marine Sciences, 31, 2, 87-92.

[7] Rao, A. D., Mourani Sinha, Neetu and Sujit Basu, 2011, Variability of Significant Wave Height over the Indian Ocean using Empirical Orthogonal Function Analysis, The International Journal of Ocean and Climate Systems, Vol. 2(2), June, pp. 75-85 (DOI: 10.1260/1759-3131.2.2.75).

[8] Sharma, R., A. Sarkar, N. Agarwal, R. Kumar, and S. Basu, 2007a, A new technique for forecasting surface wind field from scatterometer observations: Acase study for the Arabian Sea, IEEE Trans. Geoscience Remote Sensing, 45, 613–619, doi:10.1109/TGRS.2006.888093.

[9] Sharma, R., A. Sarkar, N. Agarwal, R. Kumar, and S. Basu, 2007b, Predicting wind field in the Bay of Bengal from scatterometer observations using genetic algorithm, Geophys. Res. Lett., 34, L03603, doi:10.1029/2006GL028288.

[10] WAMDI group: Hasselmann, S., K. Hasselmann, E. Bauer, P.A.E.M. Janssen, G.J. Komen, L. Bertotti, P. Lionello, A. Guillaume, V.C. Cardone, J.A.Greenwood, M. Reistad, L. Zambresky and J.A. Ewin